Basin Research (2000) **12,** 97–114

Structural and topographic evolution of the central Transverse Ranges, California, from apatite fission-track, (U–Th)/He and digital elevation model analyses

A. E. Blythe,* D. W. Burbank,*[1] K. A. Farley† and E. J. Fielding‡

*Department of Earth Sciences, University of Southern California, Los Angeles, CA 90089, USA
†Division of Geological and Planetary Sciences, California Institute of Technology, Pasadena, CA 91125, USA
‡Jet Propulsion Lab, Oak Grove Drive, Pasadena, CA 91109–8099, USA

ABSTRACT

Apatite fission-track (FT) and (U–Th)/He analyses are used to constrain the low-temperature thermal history of the San Gabriel and San Bernardino Mountains (SGM and SBM), which are part of the southern California Transverse Ranges. FT ages from 33 SGM samples range from 3 to 64 Ma. Helium ages, ranging from 3 to 43 Ma, were obtained from 13 of these samples: all of the He ages are the same or younger than their respective FT ages. FT ages from 10 SBM samples were older, ranging from 45 to 90 Ma. The FT and He data document at least three phases of cooling in the SGM, but only two in the SBM. Prior to $\sim$7 Ma, the thermal history of the SGM appears to have been nearly identical to many of the core complexes in the Basin and Range of south-eastern California: a major phase of cooling is indicated from $\sim$60 to 40 Ma, with a more recent phase beginning at $\sim$23 Ma and continuing until $\sim$10 Ma. The similarity of this timing to that of core complexes suggests that the SGM also originated as a core complex, when the rocks were adjacent to the Chocolate–Orocopia Mountains, and that some of the range-bounding faults were initially extensional. In the SBM, the two phases of cooling documented by the FT data occurred from $\sim$65 to 55 Ma, and from $\sim$18 Ma to the present. The timing on the second phase is very poorly constrained and, therefore, we do not speculate on the origin of the SBM.

The most recent phase of cooling appears to have begun at $\sim$7 Ma in the SGM, as the result of the onset of contractional deformation. A more accelerated phase of cooling may have begun at $\sim$3 Ma. Distinct variations in the total amounts and rates of cooling between different fault-bounded blocks within the SGM are documented since 7 Ma. We use these variations in cooling rates to calculate denudation rates, which are then compared to topographic characteristics for each structural block. These comparisons suggest that more rapid bedrock uplift in the eastern and southern part of the range has strongly affected the present-day physiography. Despite a higher mean elevation, the SBM are much less dissected than the SGM, suggesting that the most recent phase of cooling and bedrock uplift began in the last 3 Myr, much later than the initiation of recent bedrock uplift in the SGM.

INTRODUCTION

Low-temperature thermochronometric data, such as fission-track analyses, are commonly used to constrain the cooling history and tectonic evolution of mountain belts. Although it is relatively simple to document the cooling history of a region and to approximate the denudation history if the geothermal gradient is known, it is far more difficult to correlate that history with surface topography because a large number of variables, such as climate and rock type, can affect topography in a mountain range (Molnar & England, 1990). Despite problems, links between the surface expression of an evolving orogenic region and its exhumation history should be possible if

Correspondence: Professor Ann E. Blythe, Department of Earth Sciences, University of Southern California, Los Angeles, CA 90089, USA. Tel.: +1 213 821 1094; fax: +1 213 740 8801; e-mail: blythe@earth.usc.edu
[1]Now at: Department of Geosciences, Pennsylvania State University, University Park, PA 16802, USA.

certain conditions are met: the region must be young and it must have experienced minimal climatic variations over the time period studied. Recent studies have applied fission-track analyses to studies of the development of topography in three active mountain ranges: the Alaska Range, Southern Alps of New Zealand and Olympic Mountains of the north-western US (Fitzgerald *et al.*, 1995; Tippett & Kamp, 1995; Brandon *et al.*, 1998).

In this study, we examine the low-temperature history of the San Gabriel and San Bernardino Mountains (SGM and SBM) of southern California using a combination of apatite fission-track (FT) and (U–Th)/He (referred to here as He) thermochronology. Apatite FT thermochronology is commonly used for studying near-surface tectonic processes because it constrains thermal histories between $\sim$110 and 60 °C (Gleadow *et al.*, 1983). Helium thermochronology is a new technique that complements FT analyses in apatites and extends the low-temperature range to $\sim$40 °C (Wolf *et al.*, 1996; House *et al.*, 1999). We use FT and He data from the SGM and SBM to constrain the timing and rates of major cooling and denudation events. These databases delineate four major structural blocks in the SGM, but only a single block in the northern SBM. We then use a digital elevation model (DEM) to characterize variations in topography for the individual blocks of the SGM and to correlate these to differences in cooling and denudation rate.

GEOLOGICAL EVOLUTION OF THE TRANSVERSE RANGES

Southern California (Fig. 1) is part of the active margin between the Pacific and North American plates. The Pacific plate is moving north-westward relative to the North American plate at a rate of $\sim$5 cm yr^{-1} (DeMets, 1995). In California, this motion occurs primarily along the NNW-trending, right-lateral San Andreas fault (SAF) (Atwater, 1970). In southern California, the SAF has a more westerly trend than elsewhere along its length. Contraction along this 'big bend' in the SAF is thought to have resulted in the formation of the east–west-trending Transverse Ranges. The central Transverse Ranges (Fig. 2), which consist of the SGM and SBM, are bisected by the SAF. Although these two ranges are presently adjacent to each other, correlation of rock units suggests that the SGM originated $\sim$240 km to the SSE, near the Chocolate and Orocopia Mountains (Ehlig, 1981).

The pre-Cenozoic geological history of the SGM and SBM is similar to that of the Sierra Nevada and Salinian blocks of central California, suggesting that all of these terranes were originally part of a single Mesozoic arc complex (Barth & May, 1992). The oldest rocks exposed in the SGM and SBM are Proterozoic in age and include gneiss, amphibolite, and an anorthosite–gabbro–syenite complex (e.g. Ehlig, 1975, 1981; Barth *et al.*, 1995). In the SGM, these occur in the upper plate of the Vincent Thrust, a major north-vergent (?) structure that has been correlated to the Orocopia Thrust in the Orocopia Mountains. The lower plate of the Vincent and Orocopia Thrusts consists primarily of a schist that originated as a clastic marine sequence (e.g. Ehlig, 1981). The Vincent and Orocopia Thrusts have been interpreted to be part of a Palaeocene subduction zone (Miller & Morton, 1977; Jacobsen *et al.*, 1988; Jacobsen, 1990; Grove & Lovera, 1996).

During Mesozoic time, the Precambrian rocks of the SGM and SBM were intruded at mid-crustal levels by several large granitic bodies of at least two distinct generations, one Triassic in age and the other Late Cretaceous (e.g. Barth, 1990; Barth & May, 1992). In the eastern SGM, felsic dikes and plutons were emplaced at relatively shallow depths during late Oligocene and middle Miocene time (e.g. Miller & Morton, 1977; May & Walker, 1989). These rocks are cross-cut by a mafic dike swarm of probable middle Miocene age (Ehlig, 1981; Hazelton & Nourse, 1994).

Ingersoll & Rumelhart (1999) have proposed a three-stage evolutionary history for the Los Angeles basin, with the first two stages pre-dating significant motion on the southern SAF. During the initial phase (from 18 to 12 Ma), the western Transverse Ranges (west of the SGM) underwent transrotation. Evidence for this phase is provided by the palaeomagnetic studies of Terres & Luyendyk (1985), which have documented $37 \pm 12^{\circ}$ of clockwise rotation in the western Transverse Ranges since middle Miocene time. The second phase, from 12 to 6 Ma, was characterized by transtension. During this time period, the San Gabriel fault (a precursor of the SAF with $\sim$60 km of right-lateral offset) was active (Crowell, 1975) and sedimentation was occurring in the Los Angeles basin (Wright, 1991). The third stage, transpression, which continues today, began at $\sim$6 Ma when the southern San Andreas fault became active (e.g. Crowell, 1982; Dickinson, 1996).

Most of the exhumation of the modern-day SGM has occurred on the Cucamonga and Sierra Madre faults (see Fig. 1). Geodetic, seismic and geomorphic evidence indicates that these faults are active reverse-slip faults with a minor component of right-lateral strike-slip motion (e.g. Hadley & Kanamori, 1976; Dibblee, 1982; Savage *et al.*, 1986; Crook *et al.*, 1987; Savage & Lisowski, 1994). Palaeoseismological trench studies have recorded Holocene vertical motion of $\sim$1 mm yr^{-1} for both faults (Dolan *et al.*, 1996; Walls *et al.*, 1997). The faults are thought to flatten beneath the mountain range at depths of greater than 12–15 km (Hadley & Kanamori, 1976; Yeats, 1981; Webb & Kanamori, 1985; Ryberg & Fuis, 1998).

Geological relationships suggest that the most recent phase of bedrock uplift might have begun later in the SBM than in the SGM. On the northern margin of the SBM, the Pliocene-age Old Woman sandstone was deposited unconformably on pre-Tertiary basement and upper Miocene basalts between 7 and 3 Ma (May & Repenning, 1982; Sadler, 1982, 1993). Provenance studies

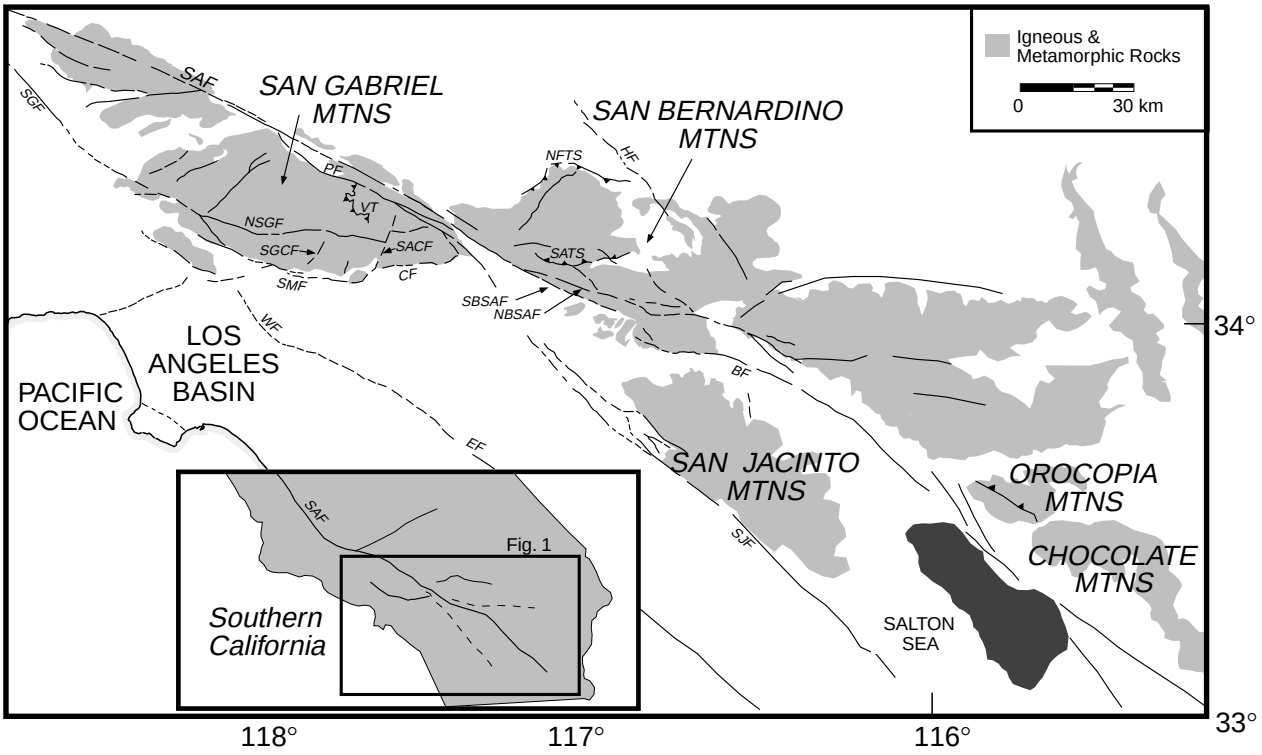

Fig. 1. Simplified map of Southern California (after Jennings, 1977). Fault names are abbreviated as follows: BF, Banning fault; CF, Cucamonga fault; EF, Elsinore fault; HF, Helendale fault; NBSAF, North Branch of the San Andreas fault; NFTS, North Frontal Thrust system; NSGF, North fork of the San Gabriel fault; PF, Punchbowl fault; SACF, San Antonio Canyon fault; SAF, San Andreas fault; SATS, Santa Ana Thrust system; SBSAF, South Branch of the San Andreas fault; SGCF, San Gabriel Canyon fault; SGF, San Gabriel fault; SJF, San Jacinto fault; SMF, Sierra Madre fault; SSGF, South fork of the San Gabriel fault; VT, Vincent Thrust; WF, Whittier fault.

indicate that only the uppermost portion of this sandstone was derived from rocks currently exposed in the SBM, suggesting that exhumation of the SBM did not begin much earlier than 3 Ma (Sadler & Reeder, 1983).

Throughout the northern SBM, a thick layer of decomposed granite is exposed and in places is covered by a veneer of gravel and late Miocene-age basalt (Oberlander, 1972). The decomposed granitic layer, which is interpreted to be a preorogenic weathering surface (Sadler & Reeder, 1983; Meisling, 1984), is now at elevations of $\sim$2500 m in the centre of the SBM. To the east, this surface is down-dropped along normal faults until exposures are found at $\sim$1000 m, the elevation of the Mojave Desert floor. The geometry of this surface, which defines the Big Bear plateau in the northern SBM, suggests that $\sim$1500 m of differential uplift relative to the Mojave Desert floor has ocurred since late Miocene time. Two active fault systems appear to be responsible for the uplift of the Big Bear plateau: the north-vergent North Frontal thrust system on the northern side (e.g. Meisling, 1984; Webb & Kanamori, 1985; Meisling & Weldon, 1989) and the south-vergent Santa Ana thrust system, which is exposed in the valley between the Big Bear plateau and the San Gorgonio block to the south. The North Frontal thrust system probably flattens at depth and may truncate the Santa Ana thrust system (Webb & Kanamori, 1985; Meisling & Weldon, 1989; Li *et al.*, 1992; Seeber & Armbruster, 1995).

APATITE FISSION-TRACK AND (U–Th)/He THERMOCHRONOLOGY

Apatite fission-track thermochronology is commonly used to determine the magnitude of cooling, exhumation and rock uplift from shallow crustal levels (e.g. Fitzgerald *et al.*, 1995; Tippett & Kamp, 1995). Fission tracks are damage zones in a crystal or glass that are formed by the fission of ^{238}U (Wagner, 1968). Although fission tracks are stable at low temperatures, they begin to shorten and disappear (anneal) with increasing temperatures (Naeser & Faul, 1969; Gleadow & Duddy, 1981). For F-rich apatites (95% of all apatites), significant annealing occurs between $\sim$60 and 110 °C at geological cooling rates (Gleadow *et al.*, 1986; Green *et al.*, 1986). This temperature range is referred to as the partial annealing zone or PAZ (Gleadow & Fitzgerald, 1987) and it forms a pseudo-stratigraphic horizon that can be used to infer the magnitude of denudation and rock uplift (Brown, 1991). The FT 'age' of a sample is commonly interpreted as the time at which the sample cooled below the closure temperature (110 °C – the upper bound of the PAZ at a cooling rate of $\sim$1–10 °C Myr^{-1}) and is determined

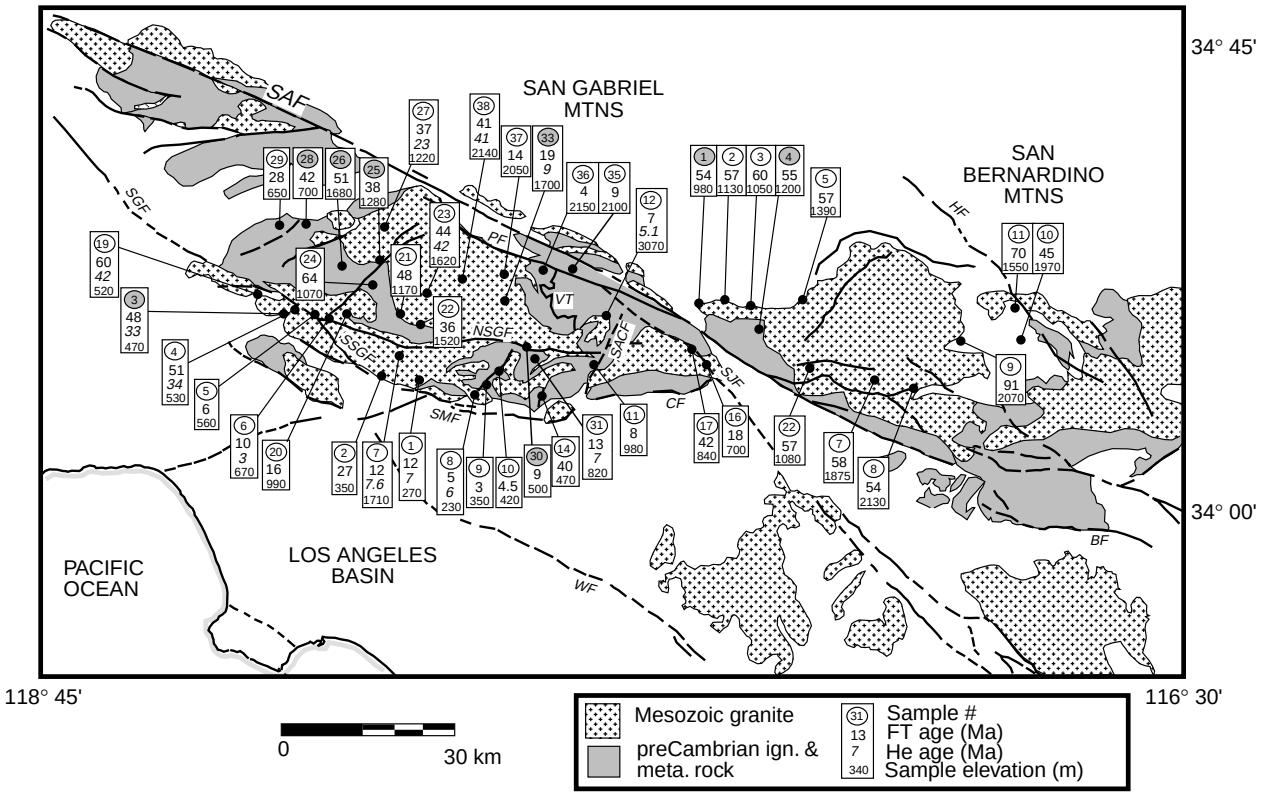

Fig. 2. Transverse Ranges map showing locations of samples and their apatite fission-track and (U–Th)/He ages. A shaded sample number indicates that a thermal model (see Fig. 4) was obtained from the track-length distribution. Geology is simplifed from Jennings & Strand (1991) and Dibblee (1982). Fault abbreviations are the same as for Fig. 1.

by measuring the density of tracks and the U concentration of the sample (Naeser, 1976).

Experimental annealing data for fission tracks in apatites (Laslett *et al.*, 1987; Carlson, 1990; Crowley *et al.*, 1991; Carlson *et al.*, 1999) provide the basis for algorithms developed to constrain the thermal history of a sample within the PAZ (Green *et al.*, 1989; Corrigan, 1991; Gallagher, 1995; Willett, 1997; Ketcham *et al.*, 1999). Thermal histories derived from these algorithms typically correlate well with other geological data, although some uncertainties exist about the extrapolation of short timescale (<1 year) laboratory experiments on annealing at temperatures below ~ 80 °C. One way to strengthen thermal models developed with track-length annealing algorithms is to use (U–Th)/He dating, which also uses the mineral apatite.

The (U–Th)/He system is based on the production of ^{4}He during U and Th series decay. Partial diffusive loss of helium from apatite occurs over temperatures of $\sim$40–90 °C (Wolf *et al.*, 1997). This temperature range, termed the 'helium partial retention zone' (PRZ), is analogous to the fission track PAZ, and can also be used as a basis for denudation estimates (e.g. House *et al.*, 1999). At a cooling rate of 10 °C Myr^{-1}, the (U–Th)/He system has a closure temperature of $\sim$75 °C (Wolf *et al.*, 1996). Thus (U–Th)/He thermochronology extends sample cooling histories to lower temperatures than FT analyses alone and can provide checks on thermal histories derived from fission track-length models.

APATITE FISSION-TRACK AND (U–Th)/He DATA

The locations and ages obtained for the samples used in this study are shown on Fig. 2. Table 1 is a summary of the FT age and length analytical data (complete analyses can be obtained from A. Blythe) and Table 2 contains the He analytical data (a description of the procedures used for He analyses can be found in Spotila *et al.*, 1998). All errors on ages quoted throughout the text are 1 sigma.

The FT length distributions were used to obtain thermal histories for eight of the 44 total samples analysed. These samples were chosen because they yielded at least 100 track-length measurements, and thus better-constrained thermal models. The measured FT length distributions were modelled using MonteTrax (Gallagher, 1995), a forward modelling program in which random time–temperature paths are generated within user-specified time–temperature bounds. The track-length distribution and 'age' predicted by each generated time–temperature path are then compared to the measured data. A genetic algorithm approach, in which several iterations of solutions are generated with each iteration more focused towards statistically significant solutions, is incorporated within the program.

Table 1. Apatite fission track analyses.

Sample	Lat., Long. Elev. (m)	No. of grains	Standard track density ($\times 10^6$ cm^{-2})	Fossil track density ($\times 10^4$ cm^{-2})	Induced track density ($\times 10^4$ cm^{-2})	Chi square prob. (%)	Fission track age (Ma)	Mean track length (μm)	Standard track dev. (μm)
San Gabriel Mountains									
Sierra Madre block									
SG-1	34°10.8′, 118°01.0′ 270	12	1.51 (2428)	4.69 (9)	95.83 (184)	96	11.8 ± 4.0		
SG-5	34°17.3′, 118°13.5′ 560	20	1.55 (2488)	8.90 (42)	313.77 (1480)	Fail	*6.1 ± 1.5		
SG-6	34°17.0′, 118°11.7′ 670	20	1.55 (2488)	7.62 (50)	189.79 (1245)	39	10.0 ± 1.4		
SG-7	34°13.5′, 118°03.3′ 1710	20	1.57 (2518)	23.32 (134)	493.82 (2838)	Fail	*11.9 ± 1.3		
SG-8	34°09.5′, 117°54.2′ 230	20	1.59 (2548)	23.30 (122)	1113.42 (5829)	39	5.3 ± 0.5		
SG-9	34°10.3′, 117°53.2′ 350	16	1.59 (2548)	1.78 (9)	148.32 (748)	79	3.0 ± 1.0		
SG-10	34°12.0′, 117°51.5′ 419	13	1.61 (2578)	4.80 (14)	275.90 (799)	96	4.5 ± 1.2		
SG-11	34°12.3′, 117°40.5′ 980	20	1.61 (2578)	5.71 (48)	175.51 (1476)	98	8.4 ± 1.2		
SG-30	34°14.0′, 117°48.3′ 500	17	2.26 (3627)	14.60 (99)	589.38 (3996)	88	9.0 ± 1.7	13.3 ± 0.2 (100)	1.71
SG-31	34°13.1′, 117°47.3′ 820	20	2.24 (3591)	11.22 (77)	309.33 (2122)	52	13.0 ± 1.5	13.7 ± 0.6 (9)	1.67
Mt. Baldy block									
SG-12	34°17.3′, 117°38.7′ 3070	20	1.63 (2608)	10.52 (67)	388.98 (2477)	20	7.0 ± 0.9		
SG-33	N34°18.7′, 117°51.6′ 1700	8	2.24 (3591)	10.50 (125)	192.86 (2295)	39	19.3 ± 1.8	12.1 ± 0.2 (100)	1.76
SG-36	34°22.2′, 117°46.0′ 2100	15	2.19 (3519)	3.08 (28)	293.95 (2672)	99	3.7 ± 0.7		
SG-37	34°21.3′, 117°51.0′ 2050	15	2.17 (3483)	11.19 (50)	274.04 (1225)	34	14.2 ± 2.1		
Western San Gabriel block									
SG-20	34°17.8′, 118°9.7′ 990	21	2.37 (3806)	8.80 (111)	207.61 (2618)	99	16.1 ± 1.6		
SG-21	34°17.7′, 118°3.5′ 1170	20	2.35 (3771)	22.15 (258)	171.93 (2003)	28	48.4 ± 3.2		
SG-22	34°16.3′, 118°1.1′ 1520	20	2.35 (3771)	70.63 (452)	575.47 (3683)	Fail	*36.3 ± 3.5	13.0 ± 0.2 (66)	1.52
SG-23	34°19.4′. 118°0.1′ 1620	14	2.32 (3735)	12.74 (106)	108.65 (904)	92	43.6 ± 4.5	13.5 ± 0.5 (5)	1.19
SG-24	34°20.2′, 118°6.6′ 1070	22	2.32 (3735)	12.14 (124)	71.01 (725)	29	63.6 ± 6.2		
SG-25	34°22.6′, 118°5.9′ 1280	20	2.30 (3699)	20.00 (242)	192.15 (2325)	24	38.3 ± 2.6	12.8 ± 0.2 (100)	1.67
SG-26	34°22.3′, 118°10.4′ 1680	20	2.30 (3699)	27.34 (231)	196.80 (1663)	10	51.2 ± 3.6	13.0 ± 0.2 (106)	1.63
SG-27	34°26.1′, 118°5.3′ 1220	12	2.28 (3663)	7.26 (60)	71.43 (590)	92	37.1 ± 4.1	13.4 ± 0.6 (9)	1.69
SG-28	34°26.4′, 118°14.6′ 700	11	2.28 (3663)	22.76 (145)	240.03 (1529)	Fail	*42.1 ± 5.4	11.6 ± 0.1 (100)	1.45
SG-29	34°26.3′, 118°17.6′ 650	18	2.26 (3627)	17.50 (56)	226.56 (725)	53	27.9 ± 3.9	13.1 ± 0.8 (3)	1.34
SG-38	34°20.9′, 117°56.0′ 2140	20	2.17 (3483)	21.31 (127)	186.87 (1078)	34	40.9 ± 3.8	14.2 ± 0.4 (7)	1.13

Table 1. (*Continued*).

Sample	Lat., Long. Elev. (m)	No. of grains	Standard track density ($\times 10^6$ cm^{-2})	Fossil track density ($\times 10^4$ cm^{-2})	Induced track density ($\times 10^4$ cm^{-2})	Chi square prob. (%)	Fission track age (Ma)	Mean track length (μm)	Standard track dev. (μm)
Tujunga block									
SG-3	34°17.5′, 118°17.2′ 470	20	1.53 (2458)	85.38 (459)	438.62 (2358)	34	47.7 ± 2.4	12.0 ± 0.1 (117)	1.45
SG-4	34°18.1′, 118°16.1′ 530	20	1.53 (2458)	43.09 (337)	193.33 (1512)	Fail	*51.2 ± 4.1	11.3 ± 0.5 (19)	2.20
SG-19	34°19.4′, 118°20.3′ 520	20	1.69 (2698)	45.10 (265)	205.10 (1205)	98	59.5 ± 4.0		
Fault sliver blocks									
SG-2	34°11.2′, 118°05.8′ 350	9	1.51 (2428)	40.32 (56)	365.06 (507)	93	26.7 ± 3.8		
SG-14	34°09.4′, 117°46.3′ 470	13	1.65 (2638)	60.35 (185)	394.70 (1210)	13	40.4 ± 3.2		
SG-16	34°12.3′, 117°27.2′ 700	23	1.67 (2668)	10.37 (94)	152.61 (1383)	18	18.2 ± 1.9		
SG-17	34°13.9′, 117°29.0′ 840	5	1.67 (2668)	45.80 (34)	289.60 (215)	91	42.3 ± 7.8		
SG-35	34°22.2′, 117°42.8′ 2150	17	2.22 (3555)	14.69 (26)	599.44 (1061)	66	8.6 ± 1.7		
San Bernardino Mountains									
SB-1	34°18.8′, 117°28.3′ 980	20	1.86 (2987)	34.35 (244)	190.88 (1356)	72	53.6 ± 3.7	12.6 ± 0.1 (106)	1.08
SB-2	34°19.5′, 117°25.9′ 1130	16	1.86 (2987)	108.70 (272)	569.45 (1425)	29	56.8 ± 3.8	9.8 ± 1.2 (2)	1.64
SB-3	34°18.3′, 117°20.3′ 1050	20	1.89 (3032)	60.54 (339)	303.93 (1702)	84	60.2 ± 3.6	13.7 (1)	–
SB-4	34°15.9′, 117°17.3′ 1200	20	1.89 (3032)	59.65 (347)	328.66 (1912)	99	54.9 ± 3.2	13.1 ± 0.1 (100)	1.03
SB-5	34°13.8′, 117°17.4′ 1390	20	1.92 (3077)	81.72 (477)	439.62 (2566)	8	57.1 ± 2.9	12.9 ± 0.6 (7)	1.45
SB-7	34°12.5′, 117°4.9′ 1875	20	1.92 (3077)	19.95 (228)	105.25 (1203)	98	58.2 ± 4.2		
SB-8	34°13.4′, 117°2.4′ 2130	9	1.95 (3121)	19.74 (60)	113.16 (344)	87	54.4 ± 7.6		
SB-9	34°15.7′, 116°56.7′ 2070	18	1.97 (3166)	51.18 (283)	177.41 (981)	97	90.9 ± 6.1		
SB-10	34°17.9′, 116°48.0′ 1970	13	1.97 (3166)	18.00 (81)	124.69 (561)	30	45.5 ± 5.4	12.9 ± 0.6 (4)	1.25
SB-11	34°20.1′, 116°49.9′ 1550	20	2.00 (3211)	47.94 (293)	217.93 (1332)	33	70.4 ± 4.5	12.8 ± 0.4 (10)	1.30
SB-22	34°20.3′, 117°13.8′ 1080	10	2.06 (3301)	45.22 (134)	259.52 (769)	74	57.4 ± 5.4	9.5 ± 1.0 (2)	1.46

All samples were processed and analysed by A. Blythe at the University of California, Santa Barbara, and the University of Southern California. Standard magnetic and heavy liquid mineral separation processes were used. Apatites were mounted in epoxy. Sample surfaces were ground and polished. Apatite mounts were etched in 7% HNO_3 at 18 °C for 22 s. An 'external detector' (e.g. Naeser, 1979), consisting of low-U (<5 p.p.b.) Brazil Ruby muscovite, was used for each sample. Samples were irradiated in the Cornell University Triga nuclear reactor. Following irradiation, the muscovites were etched in 48% HF at 18 °C for 30 min. Tracks were counted using a 100× dry lens and 1250× total magnification in crystals with well-etched, clearly visible tracks and sharp polishing scratches. A Kinitek stage and software written by Dumitru (1993) were used for analyses. Parentheses show number of tracks counted. Standard and induced track densities were determined on external detectors (geometry factor = 0.5), and fossil track densities were determined on internal mineral surfaces. Ages were calculated using zeta = 320 ± 9 for dosimeter glass SRM 962a (e.g. Hurford & Green, 1983). All ages (except those with an *) are population ages, with the conventional method (Green, 1981) used to determine errors on sample ages. The χ^2 test estimated the probability that individual grain ages for each sample belong to a single population with Poissonian distribution (Galbraith, 1981). *Central ages (Galbraith & Laslett, 1993) were used for samples that failed the χ^2 test at <5%.

Table 2.
(U–Th)/He analyses.

Sample	No. of replicate analyses	FT*	U (p.p.m.)	Th (p.p.m.)	Corrected age (Ma) ±1 sigma†
San Gabriel Mountains					
Sierra Madre block					
SG-1	1	0.72	16	19	6.56±0.66
SG-6	2	0.77	10	24	3.12±0.20
SG-7	2	0.76	27	65	7.59±0.46
SG-8	2	0.84	54	38	6.27±0.62
SG-31	2	0.71	16	6	6.79±0.41
Mt. Baldy block					
SG-12	1	0.83	20	38	5.12±0.31
SG-33	2	0.75	7	9	8.86±2.44
Western San Gabriel block					
SG-23	1	0.80	4	9	42.76±2.57
SG-27	2	0.78	3	3	23.15±1.39
SG-38	1	0.72	6	16	40.58±2.44
Tujunga block					
SG-3	3	0.86	22	45	33.25±2.00
SG-4	3	0.83	17	34	34.55±2.07
SG-19	3	0.84	14	86	42.38±2.54

* Fraction of alphas retained, see Farley *et al.* (1996). † Estimated, includes accuracy and precision of analyses.

With MonteTrax, the user specifies a composition for the apatites, the starting mean length for tracks, and the FT annealing algorithm. We used the annealing algorithm of Laslett *et al.* (1987) and a starting mean track length of 14.5 μm. The apatite composition was chosen on the basis of microprobe data from three samples, SG-4, SG-6 and SG-8. These samples were selected for microprobe analyses because they were the only samples to fail the χ^2 statistical test for single grain ages. In general, samples that pass the χ^2 test are assumed to consist of a single population of apatite with a uniform composition (Galbraith, 1981). Failure of the χ^2 test indicates that multiple populations of apatites are present. The most common cause of this effect is variation in F and Cl content (Green *et al.*, 1986). Therefore, if any variation in apatite chemistry were to exist in the Transverse Range samples, it would most likely appear in samples that failed the χ^2 test. Microprobe analyses indicated that all of the crystals in the selected three samples had an F content that was similar to or greater than Durango apatite (a common F-rich FT age standard used in annealing studies). Therefore, we have assumed that all of the samples are F-rich and a Durango apatite composition (0.4% F) was specified in the thermal modelling.

San Gabriel Mountains

The apatite FT ages from SGM samples ranged from 59.5±4.0 to 3.0±1.0 Ma. Helium ages obtained from 13 of these samples were consistently younger than the corresponding FT ages and ranged from 42.8±2.6 to 3.1±0.2 Ma. The FT and He ages are grouped according to distinct fault-bounded structural domains, referred to here as the Sierra Madre, Mt. Baldy, Western San Gabriel and Tujunga blocks (Figs 2 and 3A); this grouping is especially apparent when the ages are plotted against sample elevation (Fig. 3B).

The Sierra Madre block lies to the north of the range-bounding Sierra Madre fault and south of the northern strand of the San Gabriel fault. A break in FT and He ages across the southern strand of the San Gabriel fault (in the south-western SGM) clearly indicates that it is a significant structural boundary and, therefore, we designate the region to the west of the southern strand as the Tujunga block. The eastern boundary of the Sierra Madre block is probably formed by the NNE-trending San Antonio Canyon fault, which offsets the San Gabriel fault to the south-east of Mt. Baldy (Fig. 2). However, we do not yet have any data from the region to the east of the San Antonio Canyon fault.

The Mt. Baldy block is bounded by the San Jacinto and Punchbowl strands of the San Andreas fault zone on the north, the San Gabriel fault to the south and the San Antonio Canyon fault to the east. Its western boundary is unclear; it may be defined by a N–S fault along the nearly linear Bear Creek drainage. To the west of this drainage lies the Western San Gabriel block, which is bounded to its north by the San Andreas fault and to its south by the San Gabriel fault.

Sierra Madre block

The youngest apatite FT ages from the Sierra Madre block were from samples collected at relatively low elevations (<500 m) within the central part of the block, along San Gabriel Canyon; three samples from elevations

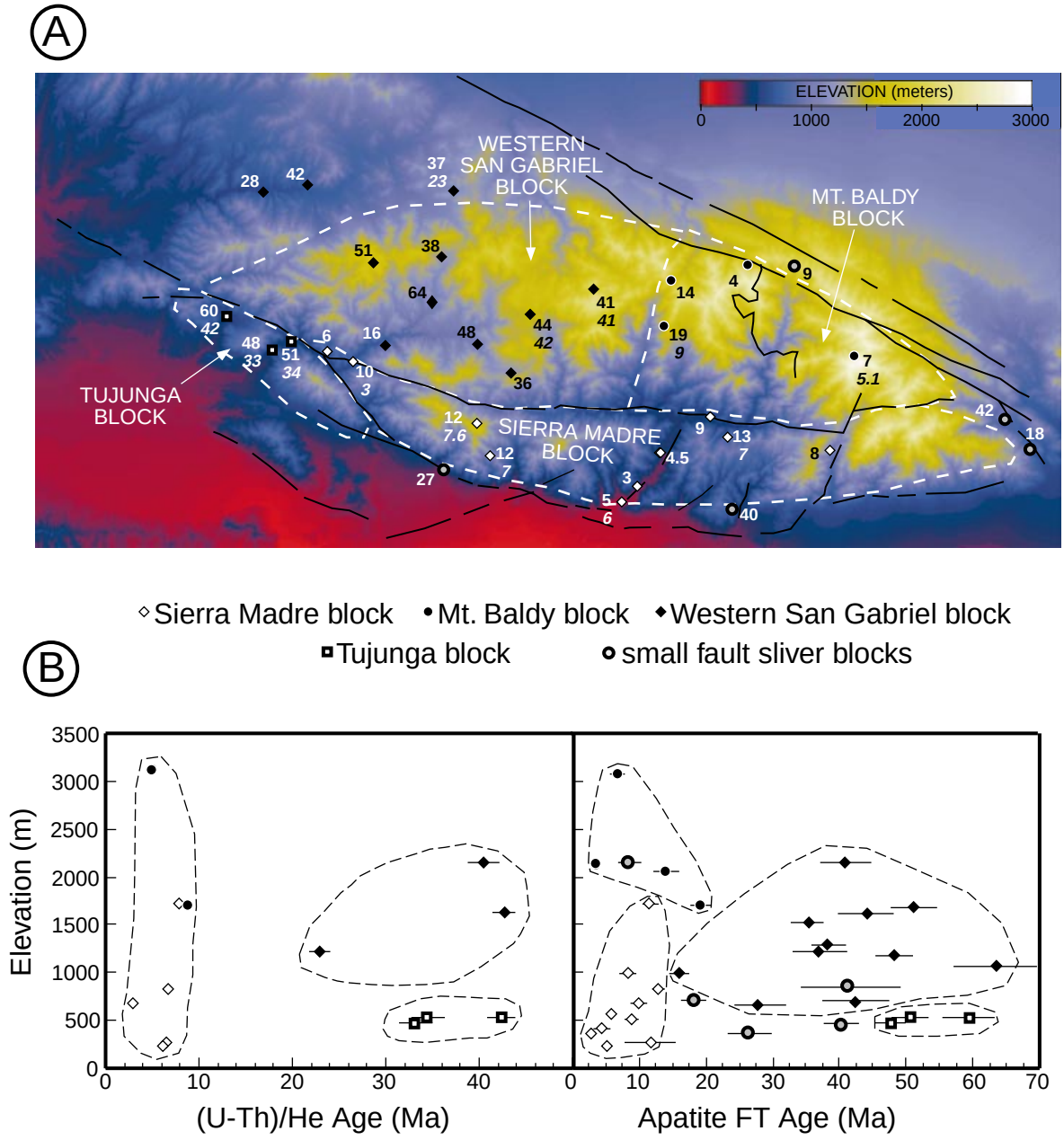

Fig. 3. (A) Thirty-metre digital elevation model (DEM) for the San Gabriel Mountains with sample locations and FT and He (in italics) ages. White dashed lines indicate the interpreted boundaries of individual blocks. Faults are shown as black lines. (B) He and FT ages are plotted vs. sample elevation. Black dashed lines show clusters of ages from individual blocks.

of 230, 350 and 419 m (SG-8, 9 and 10) yielded ages of 5.3 ± 0.5, 3.0 ± 1.0 and 4.5 ± 1.2 Ma, respectively. An He age of 6.3 ± 0.6 Ma (within one-sigma error of the FT age) was obtained from SG-8. Sample SG-30, which was collected further north in the canyon at an elevation of 500 m, yielded an older FT age of 9.0 ± 1.7 Ma. A single sample (SG-31) was collected 6 km to the east at an elevation of 820 m; this sample yielded an FT age of 13.0 ± 1.5 Ma and an He age of 6.8 ± 0.4 Ma.

Although the three youngest samples are the same age (within 2 sigma), sample SG-8 from the furthest south and the lowest elevation is the oldest (5.3 Ma). This sample yielded an He age of 6.3 Ma which together with its FT age suggests that cooling in this sample occurred earlier than in the samples from higher elevations to the north: the proximity of this sample to the range front (less than 200 m from the range-bounding fault) suggests that depression of the isotherms across the active fault may account for the older ages near the range front. The other four samples show an increase in FT age with increasing elevation (shown in Fig. 3B). The modelled thermal history derived from the track-length distribution of sample SG-30 indicates rapid cooling from 10 to 6 Ma, followed by somewhat slower cooling from 6 Ma to the present (Fig. 4). Samples collected elsewhere in the Sierra Madre block are consistent with the San Gabriel Canyon

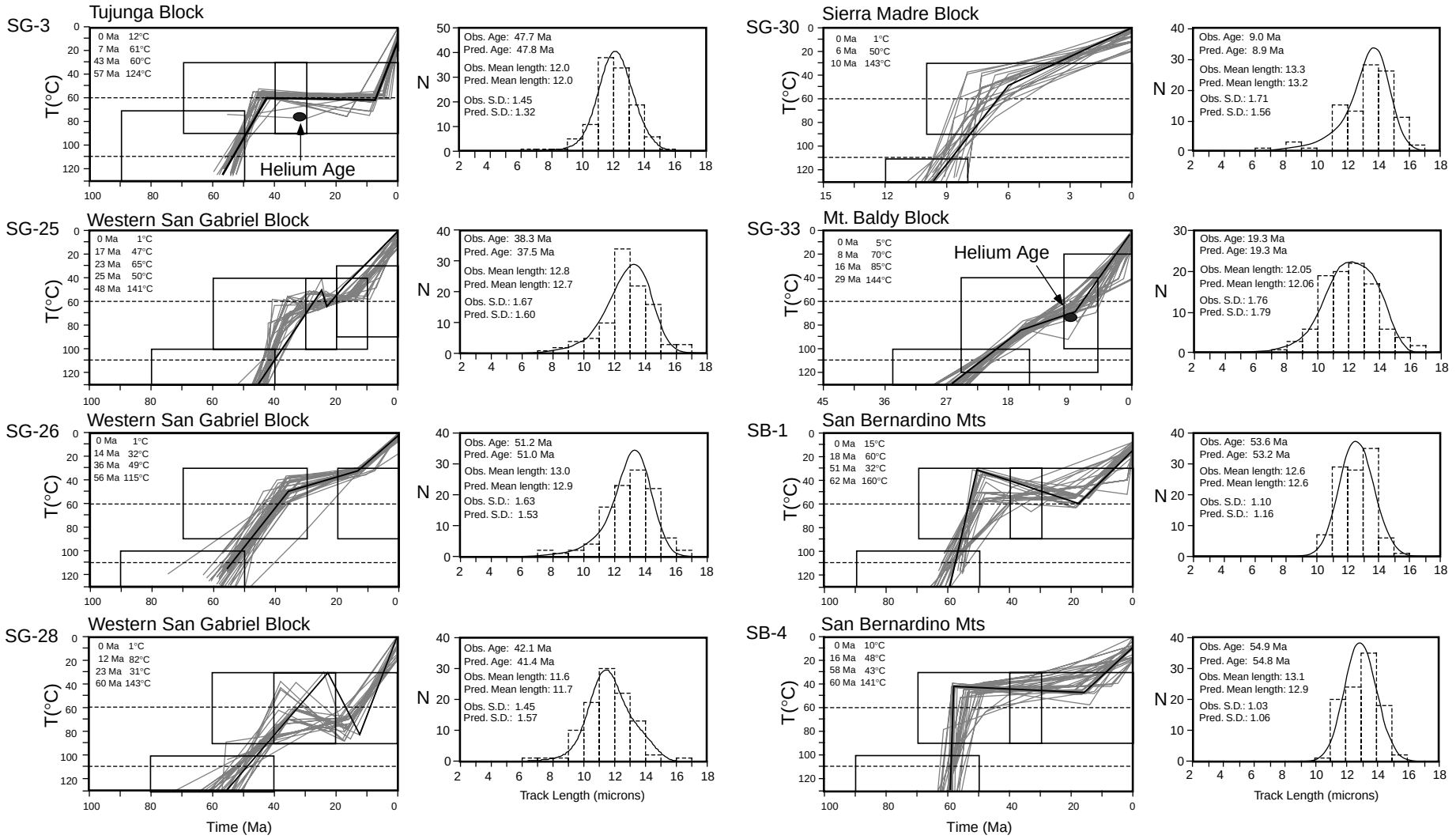

Fig. 4. Thermal models obtained from track length distributions. The time–temperature bounds chosen for each sample are shown as black boxes on each plot; the input into the thermal-history models also included the modern-day mean annual surface temperature of 10 ± 10 °C. The grey lines on each time–temperature history represent solutions that statistically matched the observed data. The black line is the 'best-fit' solution for the sample. The adjacent plots compare the observed track-length distribution (shown as the dashed histogram) with the predicted distribution (shown as a black line) for the best-fit solution.

results. Significantly older FT ages of 26.7 ± 3.8 and 40.4 ± 3.2 were obtained from two samples (SG-2 and 14) collected at low elevations (350 and 470 m) within 100 m of the topographic range front, where several splays in the active fault occur. These samples probably have older ages because they were collected from minor fault block slivers that had undergone far less vertical displacement than the main splay of the Sierra Madre fault. Thus, we will not consider them part of the Sierra Madre block.

The youngest He age of 3.1 ± 0.2 Ma from SG-6, collected in the westernmost part of the block, suggests that the western part of the range might have undergone a greater amount of total cooling in the last 3 Ma than the rest of the block (where He ages were consistently older). However, more He analyses are needed to confirm this.

Western San Gabriel block

Ages ranging from 16.1 ± 1.6 to 63.6 ± 6.2 Ma were obtained from samples collected in the north-western part of the SGM. The oldest ages (63.6 and 51.2 Ma) are from samples SG-24 and 26 collected near the middle of the block. Two samples from the eastern part of this block, SG-23 and 38, have He ages of 42.8 ± 2.6 and 40.6 ± 2.4 Ma that are indistinguishable from their FT ages of 43.6 ± 4.5 and 40.9 ± 3.8 Ma. This overlap in ages is consistent with rapid cooling through the combined PAZ and PRZ occurring at that time. Sample SG-27, collected to the north-west of these two samples, yielded FT and He ages of 37.1 ± 4.1 and 23.2 ± 1.4 Ma, suggesting a longer residence within the PRZ and slower cooling from FT to He temperature ranges.

Thermal models based on the track-length distributions were obtained from three samples, SG-25, -26 and -28, which had ages of 38, 51 and 42 Ma, respectively (Fig. 4). Two distinct cooling phases can be seen in these models: all three samples are predicted to have cooled rapidly prior to ~ 40 Ma, which is consistent with the coincident FT and He ages of samples SG-23 and 38. The thermal model for sample SG-28 predicts cooling from ~ 80 °C over the last 12 Myr. Models for the other two samples predict a smaller total cooling (of ~ 50 °C) over the last ~ 17 Myr, although the modelling is considerably less reliable at these lower temperatures.

Tujunga block

South-west of the southern San Gabriel fault, three samples (SG-19, 3 and 4) were collected at elevations of 520, 470 and 530 m, respectively. These samples yielded significantly older FT ages (59.5 ± 4.0, 47.7 ± 2.4 and 51.2 ± 4.1 Ma) and He ages (42.4 ± 2.6, 33.3 ± 2.0 and 34.6 ± 2.1 Ma) than samples from the Sierra Madre block.

The modelled thermal history for sample SG-3 indicates cooling from ~ 120 to 60 °C occurred from ~ 57 to 43 Ma, followed by thermal stasis until ~ 7 Ma, when cooling to the present-day surface temperature occurred (Fig. 4). This sample yielded an He age of 33.3 Ma, which is older than would be expected with the modelled thermal history, and is more consistent with residence at a temperature of ~ 50 °C or less from 43 to 7 Ma.

Mt. Baldy block

The youngest FT age (3.7 ± 0.7 Ma) from the Mt. Baldy block came from sample SG-36, which was collected adjacent to the Punchbowl fault. Young FT and He ages of 7.0 ± 0.9 and 5.1 ± 0.3 Ma, respectively, were obtained from the top of the highest peak (Mt. San Antonio or, more commonly, Mt. Baldy, at ~ 3070 m) in the SGM. West of Mt. Baldy, FT ages are older: two samples (SG-33 and 37) collected north of San Gabriel Canyon yielded FT ages of 19.3 ± 1.8 and 14.2 ± 2.1 Ma. Thermal modelling of the track-length distribution of SG-33 predicts cooling from 130 to 70 °C from 29 to 9 Ma, followed by more rapid cooling at ~ 8 Ma (Fig. 4). The He age of 8.9 ± 0.7 Ma from this sample, if interpreted as the time of cooling through 75 °C, is consistent with this thermal model.

Blocks adjacent to the San Andreas Fault

Two samples (SG-16 and 17) were collected from the block between the San Jacinto and San Andreas faults; these samples yielded FT ages of 18.2 ± 1.9 and 42.3 ± 7.8 Ma, respectively. SG-35, collected between the Punchbowl and San Andreas faults, yielded a younger FT age of 8.6 ± 1.7 Ma.

San Bernardino Mountains

The FT ages from the SBM ranged from 45.5 ± 5.4 to 90.9 ± 6.1 Ma. Eight ages from the north-western and south-central parts of the range are remarkably consistent, varying from 53.6 ± 3.7 to 60.2 ± 3.6 Ma, with a mean age of 57 Ma. The SBM FT ages were similar to He ages of 64–20 Ma obtained in a previous study of this part of the SBM (Spotila *et al.*, 1998). Thermal models derived from the track-length distributions for samples SB-1 and SB-4 are shown in Fig. 4. Both of these samples were consistent with 60–70 °C of cooling from ~ 60 to 50 Ma (at a rate of 5–10 °C Myr^{-1}), followed by thermal stasis and/or a slight reheating, with a pulse of more rapid cooling from temperatures of ~ 50 and 40 ± 10 °C, respectively, from 20 ± 15 Ma until present-day surface temperatures are reached (at a rate of 2–5 °C Myr^{-1}). Although the best-fit solutions to both models indicate a second phase of more rapid cooling from 18 to 16 Ma to the present, the temperatures represented are too low for this part of the thermal model to be considered very reliable.

Three samples yielded FT ages that were significantly different from the eight samples described above. The oldest FT age, 90.9 ± 6.1 Ma, is from a relatively high

elevation (2073 m) in the central part of the range (sample SB-9). Ages of 45.5 ± 5.4 and 70.4 ± 4.5 Ma were obtained from samples SB-11 and 10 collected near the NNE-trending Helendale fault. These last three sample ages suggest that multiple phases of Mesozoic cooling might be present in the SBM, but additional study is needed to confirm this.

INTERPRETATION

The FT and He data presented above constrain sample thermal histories between ~ 120 and 45 °C, the boundaries of the combined apatite PAZ and PRZ. The best-constrained thermal histories are from samples SG-3 and SG-33, which yielded both FT and He ages, as well as thermal models based on track length measurements. Interpretations of denudation, exhumation, bedrock uplift and topography, respectively, from thermal data require a progressive number of assumptions about geological conditions in the past. For the simplest case, denudation amounts can be estimated from thermochronological data by making assumptions about the geothermal gradient. The present-day geothermal gradient in southern California is ~ 25–35 °C km^{-1} (Wright, 1991), although it has probably not been stable through time. During Miocene time, voluminous volcanics were extruded throughout the Basin and Range, as well as in the SGM and SBM, suggesting that the geothermal gradient in the study area may have been significantly higher, perhaps > 40 °C km^{-1} (e.g. Foster *et al.*, 1993). Therefore, large uncertainties are associated with conversions of cooling estimates to denudation amounts prior to ~ 10 Ma. Consequently, we will limit our denudation estimates to the interval from 10 Ma to the present. Exhumation, which is distinguished from denudation by including tectonic processes such as extensional faulting, also requires assumptions about geothermal gradient, as well as knowledge of the geometry of relevant faults. Bedrock uplift, defined as the upward motion of a column of rock relative to the geoid, is more difficult to extract from thermochronological data because a topographic reference frame is needed (Molnar & England, 1990). Topographic relief can greatly disturb near-surface isotherms, leading to overestimations of denudation rates and bedrock uplift (Stüwe *et al.*, 1994; Mancktelow & Grasemann, 1997). The rate of erosion, however, must be quite high (> 5 mm yr^{-1}) for this effect to be significant, and it is unlikely that such high rates occurred in the Transverse Ranges during the last 10 Myr.

With these caveats in mind, we begin by interpreting the cooling histories of the SGM and SBM from the FT and He data. The data appear to delineate three major phases of Cenozoic cooling. In the SGM, the oldest phase of cooling documented by the FT data is seen at ~ 60 Ma in the Tujunga and Western San Gabriel blocks. This time, which dates cooling through ~ 110 °C, appears to be related to deformation along the continental margin, as indicated by the formation of the Vincent and Orocopia Thrusts. $^{40}Ar/^{39}Ar$ data from K-feldspars document cooling in the hangingwall of the Vincent Thrust (part of our Mt. Baldy block) at a similar time, from ~ 60 to 55 Ma (Grove & Lovera, 1996).

Cooling that was in progress at ~ 60 Ma appears to have continued until ~ 40 Ma in the Western San Gabriel block. In the eastern part of the block, rapid cooling from ~ 110 °C to 40 °C at ~ 44–40 Ma is indicated by the coincidence of FT and He ages from two samples. The exact cause of this accelerated cooling at ~ 40 Ma is unclear: one possibility is that it was caused by rock uplift and erosion as the result of the impingement of the Pacific–Farallon spreading centre on the California margin: the onset of rapid deposition of the nonmarine Sespe formation in localized basins in southern California during late Eocene time supports this idea (Nilsen, 1987).

The second phase of cooling appears to begin during late Oligocene to early Miocene time. This cooling event is represented by Miocene FT ages distributed throughout the Sierra Madre and Mt. Baldy blocks and from the southern edge of the Western San Gabriel block (Figs 2 and 3). The strongest evidence for this cooling comes from track-length modelling of samples SG-30 and 33, which reveal significant Miocene cooling (Fig. 4). Ten other samples from the SGM yielded FT ages between 20 and 7 Ma. Track-length models for both samples SG-30 and SG-33 indicate fairly simple cooling histories over the last 10 and 23 Myr, respectively, with no indication of complicated reheating events, such as might be expected if the cooling were the response to waning Miocene volcanism.

We therefore interpret these 10 FT ages as cooling ages associated with a change in the style of tectonism within the SGM. Although some of this cooling may be the result of a simple decrease in the geothermal gradient during mid-Miocene time, we interpret most of it to have resulted from extensional exhumation and we suggest that the San Gabriel Mountains originated as a core complex. We base this interpretation on the similarities in timing with that obtained from metamorphic core complexes in south-eastern California, such as the Piute Mountains (Foster *et al.*, 1991, 1993; Scott *et al.*, 1998), as well as the timing proposed by Crouch & Suppe (1993) for extension in the Los Angeles Basin.

Although they did not specifically deal with the San Gabriel Mountains, Crouch & Suppe (1993) suggested that the Los Angeles Basin and surrounding Borderlands had experienced a significant amount of Oligocene–Miocene extension. Using seismic reflection profiles and existing geological data, they interpreted several of the major strike-slip faults that transect the Los Angeles basin region, such as the Newport–Inglewood fault, as reactivated from steeply dipping normal faults. Similarly, we suggest that the Sierra Madre and San Gabriel faults were originally south-dipping normal faults with relatively steep dips (Fig. 5). In this scenario, these two faults would have to have undergone significant rotation

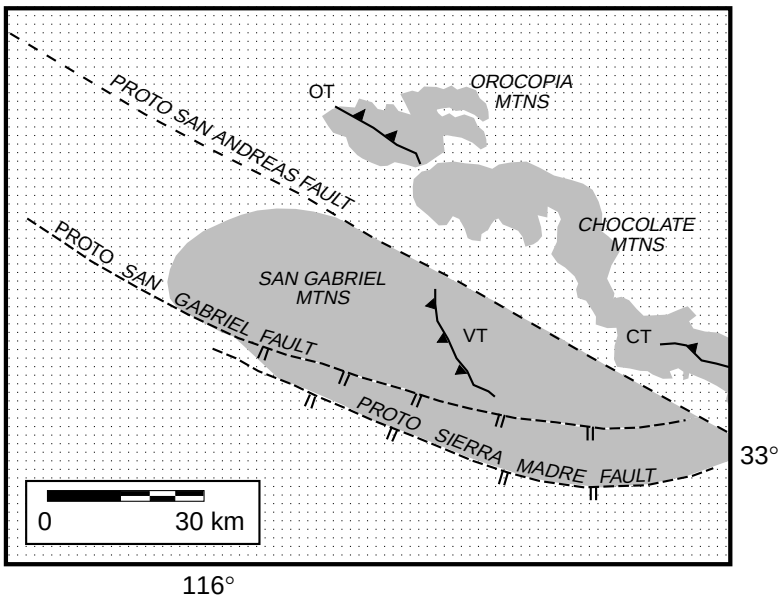

Fig. 5. Speculative reconstruction of the San Gabriel Mountains during middle Miocene time. Ticks on faults are on the hangingwall side. See text for discussion.

to reach their present-day orientations: no independent geological evidence exists to support this suggestion.

At ~12 Ma, the San Gabriel fault began to accommodate right-lateral slip (Crowell, 1975). The total amount of slip on the northern strand of the San Gabriel fault, which forms the northern boundary of the Sierra Madre block, is ~22 km. Slip on the northern strand had ended by 5 Ma, and possibly considerably earlier if the slip on the two strands of the San Gabriel fault was not simultaneous, but instead occurred sequentially. The southern strand of the San Gabriel fault accounts for 38 km of the total slip, although the exact location of the southern strand of the San Gabriel fault is unclear. If a constant slip rate is assumed and the slip on the two strands was sequential, the transfer of slip from northern to southern strands would have occurred at ~8 Ma.

This timing is convenient for our interpretation of a more rapid phase of cooling in the SGM beginning at ~7 Ma as indicated by He data from the Sierra Madre block (with no correlation between age and elevation) and the FT age from the top of Mt. Baldy. We interpret this cooling to have been caused by bedrock uplift and erosion as the result of the onset of contraction in the SGM. Supporting evidence is seen in sedimentation patterns in the Los Angeles basin (Wright, 1987, 1991) where, at ~7 Ma, the first northerly derived sediments were deposited. At this time the Sierra Madre fault was probably reactivated as a reverse fault with a substantial component of north-side-up dip-slip motion. The San Gabriel fault appears to have had some vertical offset along it in the last 7 Myr, as indicated by the juxtaposition of younger ages (than 7 Ma) on the south side and older ages on the north side of the fault (this is particularly apparent in the westernmost part of the block).

The San Bernardino Mountains appear to have a different thermal history from the SGM. The initial phase of cooling documented by the FT data occurred from ~60 to 50 Ma, with ~60 °C of cooling during this time period. This timing is consistent with the Laramide cooling event seen throughout the western USA, which may have been caused by rock uplift and erosion, or a decrease in the geothermal gradient associated with flat-slab subduction (Dumitru *et al.*, 1991). In the SBM, thermal stasis or slow cooling appears to have followed the Laramide cooling (Fig. 4). Although the thermal models from track-length distributions appear to indicate an increase in the rate of cooling at ~18 Ma, the temperatures at that time were too low for reliable interpretation based on fission-track lengths. Therefore, we do not attempt to interpret the latest phase of Miocene cooling in the SBM.

Deunudation rates and topographic characteristics of the SGM

High elevations and steep slopes in a mountain range are generally recognized as an indication of recent bedrock uplift and high denudation rates. However, only a few recent studies have directly compared topographic characteristics with denudation rate (e.g. Tippett & Kamp, 1995; Burbank *et al.*, 1996). These studies were of the Southern Alps of New Zealand and the northwest Himalayas, respectively, both of which have relatively high precipitation rates. We use the FT and He data from each of the blocks within the SGM, an area with much lower precipitation rates, to calculate cooling and denudation rates over the last 7 Myr. These rates can then be compared to the slope distributions and average rainfall of each structural block in order to make some general observations.

Within the SGM, variations in the total amounts of bedrock cooling are seen over the last 7 Myr for the individual structural blocks. These variations in cooling rate can be used to determine variations in denudation rates between the structural blocks by estimating the

temperature for each block at 7 Ma and using a fixed geothermal gradient of 25 °C km^{-1}. For FT and He ages younger than ~10 Ma, we will assume that the ages represent cooling through closure temperatures of 110 and 75 °C, respectively. For older ages, these assumptions are still generally applicable (see Fig. 4), although they become less reliable as the age of the sample increases, and the thermal history becomes more complicated.

The highest cooling and denudation rates in the SGM since 7 Ma have occurred in the Sierra Madre and Mt. Baldy blocks, which have the youngest FT and He ages. One way to reconstruct cooling histories that are variable through time is to use both FT and He thermochronometers at a single site. Where paired data are present in this study, changes in the apparent cooling rate through time can be defined. For most of the sites in the Sierra Madre block, for example, average cooling rates between 13 and 7 Ma were 5–6 °C Myr^{-1}, whereas from ~7 Ma to the present, they were nearly twice as rapid. Four He ages from the Sierra Madre block ranged from 6.3 to 7.6 Ma, indicating a cooling rate of ~10 °C Myr^{-1} and a denudation rate of ~0.4 km Myr^{-1}.

The samples collected in San Gabriel Canyon, which show a correlation between elevation and FT age, suggest that there might have been a two-phase cooling history, with slower cooling from ~13 to 3–4.5 Ma, followed by more rapid cooling until the present. Based on the young FT ages (3 and 4.5 Ma), cooling and denudation rates of >25 °C Myr^{-1} and ~1 km Myr^{-1} are calculated from 3 Ma to the present. The He age (3.1 Ma) from the westernmost sample (SG-6) collected in this block yields a similar rate. The acceleration of cooling and erosion at 3 Ma may date the onset of the ongoing 'Pasadenan Orogeny' when significant shortening began in the Transverse Ranges (Yeats, 1981).

The cooling and denudation rates estimated for the Mt. Baldy block are similar to those of the Sierra Madre block. Sample SG-36, which was collected at an elevation of 2100 m, yielded an FT age of 3.7 Ma and estimated cooling and denudation rates of ~25 °C Myr^{-1} and ~1 km Myr^{-1}. Sample SG-12, from an elevation of 3000 m, yielded FT and He ages of 7 and 5.1 Ma; these ages are consistent with cooling and denudation rates of ~15 °C Myr^{-1} and 0.6 km Myr^{-1}. A major difference between the Sierra Madre block and Mt. Baldy block samples, however, is the elevations at which the samples were collected; the significantly higher elevations of the young samples in the Mt. Baldy block (2–3 km) vs. those of the young samples in the Sierra Madre block (<0.5 km) suggest that this block has undergone more bedrock uplift even though the denudation rate is similar. If this is true, and if it is further assumed that the blocks initially had similar elevations before deformation, this would imply that the mean elevation of the Mt. Baldy block should be proportionally higher than that of the Sierra Madre block, and indeed such a difference is apparent: 1690 m vs. 1098 m, respectively.

Cooling and denudation rates from the Western San Gabriel block initially appear to be significantly lower than those found to the east and south. Most of the FT ages are >40 Ma, which if taken at face value imply cooling rates of ~3 °C Myr^{-1} and denudation rates of <0.1 km Myr^{-1}. Modelling of the track-length distributions, however, suggests a rather different interpretation. These models indicate that, following cooling below 110 °C in the early Cenozoic, the rocks either remained at a fairly constant temperature or cooled very slowly for 10–30 Myr, whereas cooling rates accelerated to ~8–10 °C Myr^{-1} from late Miocene to the present. In the context of this relatively rapid cooling, the early Cenozoic FT ages indicate that the total amount of denudation since 10 Ma is likely to be considerably less in the western San Gabriels than in the Mt. Baldy and Sierra Madre blocks. A similar interpretation can be made for the Tujunga block. Although FT ages in the block are all older than 40 Ma, thermal modelling of track lengths (Fig. 4) indicates relatively rapid cooling (~9 °C Myr^{-1}) since 7 Ma.

There are significant contrasts in topographic characteristics between the four SGM blocks. Mean elevations, mean hillslope angles and mean hillslope relief are calculated from the 30-m digital elevation model or DEM (compiled from USGS data sets) of the region (Table 3, Figs 6 and 7). Previous studies (Ahnert, 1970, 1984; Pinet & Souriau, 1988) have suggested that relief in a moutain belt is correlated with erosion rate. It is also commonly assumed that rapid erosion rates are associated with high elevation and steep slopes. As slopes increase in steepness, rates of downslope transport will also increase, depending on the dominant hillslope mechanism. Determination of a widely applicable threshold slope angle for failure by bedrock sliding is difficult due to differences in rock strength, jointing, climate and vegetation. Nonetheless, when the mean slope angle is similar to or greater than the angle of repose for many noncohesive materials (~30°), the landscape is probably at or near the threshold for slope failure (Schmidt & Montgomery, 1995).

Mean slope angles in both the Mt. Baldy block (~29°) and the Sierra Madre block (~28°) are sufficiently steep to suggest that many slopes are hovering near the critical angle for failure by landslides (Fig. 7; Table 3). In contrast, lower mean slope angles in the Western San Gabriel block (~24°) and the Tujunga block (~25°) indicate that fewer slopes are near that limit. The

Table 3. Topographic characteristics within the San Gabriel Mountains.

Region	Mean elevation (m)	Mean relief (m)	Mean slope angle (°)
Mt. Baldy	1690	242	29.3
Sierra Madre	1098	214	28.1
Tujunga	858	199	24.9
W. San Gabriel	1422	176	24.3

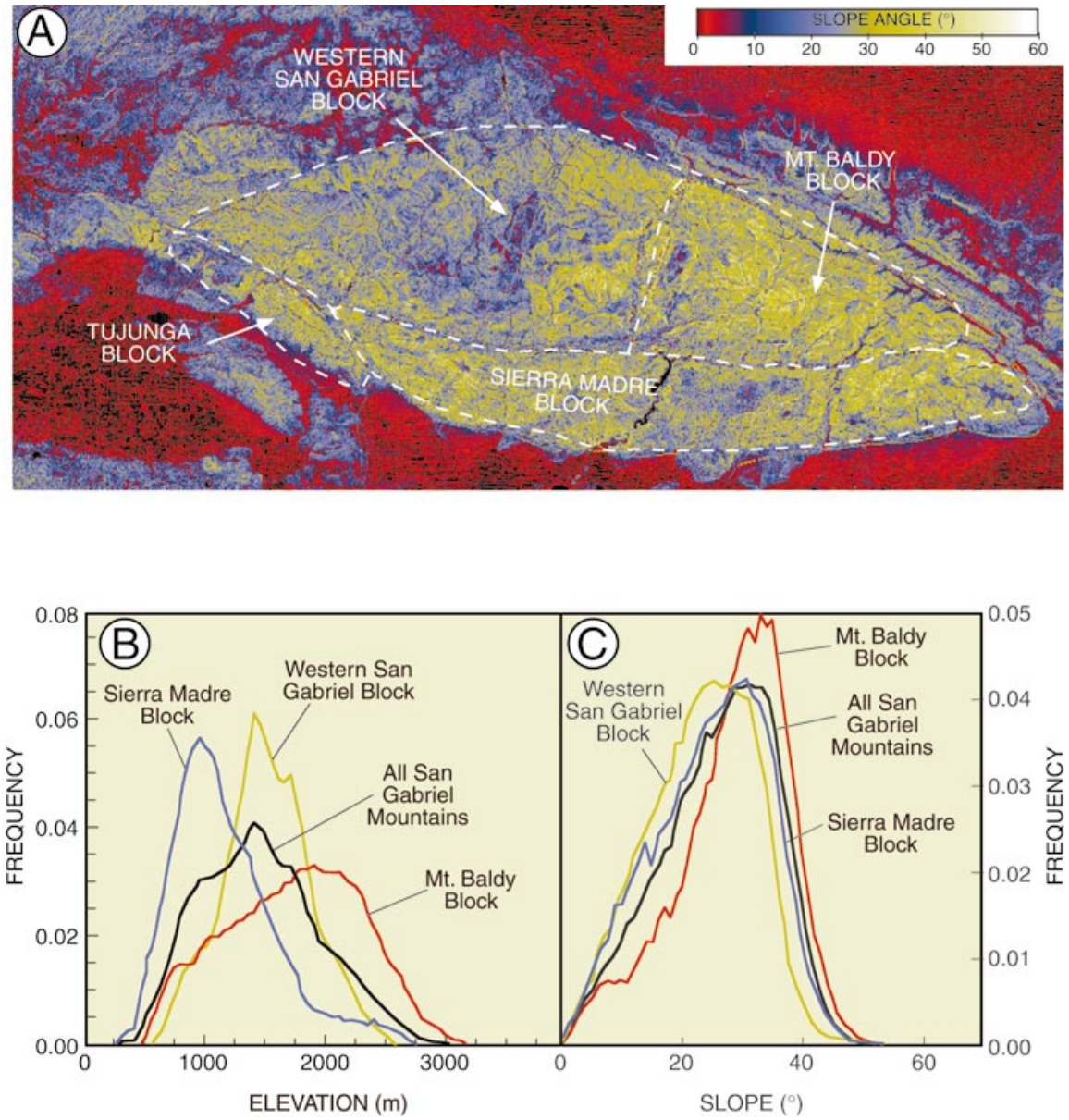

Fig. 6. (A) Slope map, (B) hypsometry and (C) slope distributions for the San Gabriel Mountains. The hypsometry and slope distributions for the three largest blocks (Mt. Baldy, Sierra Madre and Western San Gabriel) are compared with those for the entire SGM. See text for discussion.

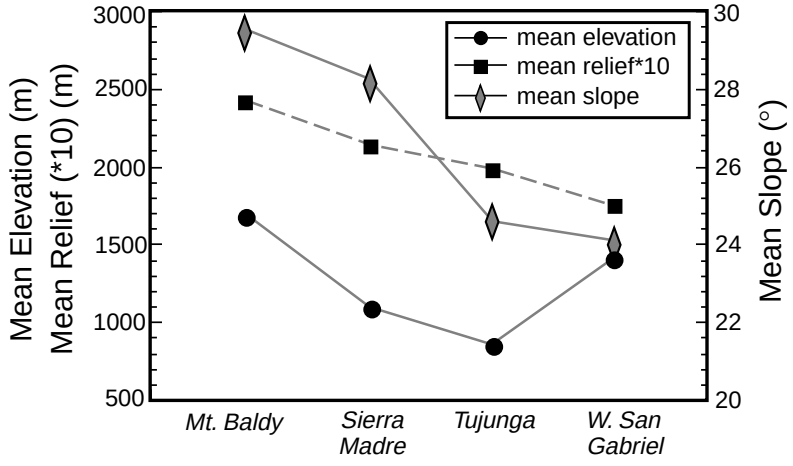

Fig. 7. Graph showing the relationship between mean elevation, relief and slope for the San Gabriel Mountain blocks.

contrasts among these four blocks mimic the trends indicated by the cooling data in that the Mt. Baldy and Sierra Madre blocks have experienced the highest rates of denudation. Despite the differences between blocks, the mean slope angles of $>20^{\circ}$ in all four areas indicate geomorphically rugged topography and rapid denudation consistent with relatively rapid cooling (>8–$10\ ^{\circ}C\ Myr^{-1}$) during the past 7 Myr.

Hillslope relief is also relevant to processes such as landsliding. Hillslope relief can be calculated as the difference between the elevation of each pixel in a block and the elevation of the nearest stream valley at the base of the slope. The mean relief calculated here represents an average across all pixels in a block (Fig. 7). The variations in mean relief between blocks mimic those of mean slope angles, with the highest mean hillslope relief found in the Mt. Baldy block and significantly less relief (by 35%) in the Western San Gabriel block. In combination with the steeper hillslopes in the Mt. Baldy and Sierra Madre regions, the relief measurements reinforce the interpretations of contrasts in denudation rates among different blocks.

Mean elevation, however, does not mimic the observed differences in cooling rates, slope angles, or relief. The Western San Gabriel block has a mean elevation approaching that of the Baldy block (Fig. 7) even though all other data sets indicate that it is eroding less rapidly than the other blocks. We interpret this decorrelation between mean elevation and denudation rate to indicate that rates of rock uplift have outpaced rates of erosion, and therefore the mean elevation of the block has increased. This conjecture is consistent with the observation that the northern half of the Western San Gabriel block displays low relief, low slope angles and a consistent mean elevation: all characteristics of a formerly low-relief surface that has undergone relatively recent bedrock uplift. This region is analogous to the Big Bear plateau in the northern San Bernardino Mountains, where another uplifted, low-relief surface is preserved (Spotila *et al.*, 1998) and shows similarly low slopes and high mean elevation.

Regional variations in relief, slope angles and mean elevation are caused by the interactions between tectonics, surface processes and climate. River spacing can also exert control on the mean relief and elevation (Meigs *et al.*, 1999; Sugai & Ohmori, 1999). The courses of rivers in the landscape, however, are often influenced by the geometry of structural features. Blocks that experience rock uplift, but have few faults, will tend to erode more slowly. Where there are pre-existing weaknesses to exploit, rivers will erode rapidly headward along these weaknesses and will maximize hillslope relief along their valleys. In the eastern and southern SGM, deep valleys along the trace of the San Gabriel fault, and NNE-trending faults (including the San Antonio Canyon fault) help to generate high relief along adjacent hillslopes and along tributaries which are graded to these fault-controlled valleys. In contrast, in the north-western San Gabriel and San Bernardino Mountains, there are few catchments containing large, low-gradient rivers that would enhance hillslope relief and denudation in these regions.

CONCLUSIONS

A substantial database consisting of apatite fission-track and (U–Th)/He analyses was obtained from the SGM and SBM of Southern California. These thermochronometric data were used to constrain the timing and geometries of major deformational events. In addition, a DEM was used to examine the topographic characteristics of the SGM since 7 Ma. Our major conclusions are:

1 The earliest phase of cooling seen in the SGM began at ~ 60 Ma and continued through 40 Ma. The earliest part of this cooling is probably a continuation of the Laramide cooling event seen throughout the Cordillera, and a more accelerated phase of cooling at ~ 40 Ma may be related to the impingement of the Pacific–Farallon spreading centre on the California margin at this time.

2 A significant period of cooling in the SGM appears to have begun at ~ 23 Ma. This timing is very similar to a period of extensional exhumation in the southern Basin and Range, leading us to suggest that extensional exhumation is likely to have occurred in the SGM at this time also, when the SGM were adjacent to the Chocolate and Orocopia Mountains. If so, then many of the SGM range-bounding faults, such as the Sierra Madre and Cucamonga faults, may well have originated as normal faults. This origin would help to explain the steep dip ($\sim 55^{\circ}$) of the Sierra Madre fault. This suggestion is significant because it implies that the Colorado River corridor of extension was wider than previously thought. Crouch & Suppe (1993) have previously suggested that the Los Angeles basin underwent significant extension at this time; the FT data from this study provide evidence that the SGM were part of this overall pattern of extension and core complex formation. Cooling related to this event appears to have continued until ~ 12 Ma.

3 Cooling appears to have accelerated at ~ 7 Ma in the SGM. We suggest that this is the time that contraction began in the SGM, when the range-bounding Sierra Madre fault became active as a reverse fault.

4 The cooling rate may have increased again at ~ 3 Ma in the SGM, but more data are needed to confirm this.

5 The SGM can be divided into four distinct blocks which appear to have different cooling and denudation rates over the last 7 Myr. The highest denudation rates ($\sim 1\ km\ Myr^{-1}$) in the SGM have occurred in the last 3 Myr in the Mt. Baldy block (the north-eastern block, which includes the highest peak) and the Sierra Madre block (the range front between the Sierra Madre and San Gabriel faults). The Mt. Baldy block has the highest average slopes in the SGM (calculated with a DEM) and the highest average elevations, as would be expected from the area with the highest denudation rates. The lowest denudation rates over the last 7 Myr (and the lowest

slopes) are seen in the Western San Gabriel and Tujunga blocks in the western and north-western parts of the range. The Sierra Madre block, however, which had denudation rates that were as high as those in the Mt. Baldy block, had significantly lower slopes and average elevations. We suggest that variations in the timing of initiation of bedrock uplift along individual faults as well as variations in bedrock uplift rates between blocks are controlling the physiography of the SGM.

6 Two phases of cooling are seen in the SBM: the earliest is from ~65 to 55 Ma (the Laramide event) and the latest, which is poorly documented here, may have begun at ~18 Ma. The SBM have undergone far less denudation in the last 10 Myr than the SGM; this is probably because contraction began very recently in the SBM (in the last few milllion years).

7 In general, the FT and He data indicate similar thermal histories for samples, especially those with younger ages. However, there was some discrepancy in the thermal history predicted by the two methods for one sample, SG-3, suggesting that some refinement is needed in either the fission track annealing or He retention equations for time periods of more than ~20 Myr.

ACKNOWLEDGMENTS

This project was funded by NASA grant (NAG-5-2191) to D. Burbank and a Packard Fellowship to K. Farley. L. Moresi and W. Featherstone assisted with sample collection on Mt. San Antonio (Mt. Baldy). Reviews by A. Densmore and F. Stuart were helpful and greatly appreciated, as were comments by A. Barth.

REFERENCES

Ahnert, F. (1970) Functional relationships between denudation, relief, and uplift in large mid-latitude basins. *Am. J. Sci.*, **268,** 243–263.

Ahnert, F. (1984) Local relief and the height limits of mountain ranges. *Am. J. Sci.*, **284,** 1035–1055.

Atwater, T. (1970) Implications of plate tectonics for the Cenozoic tectonic evolution of western North America. *Bull. Geol. Soc. Am.*, **81,** 3513–3536.

Barth, A.P. (1990) Mid-crustal emplacement of Mesozoic plutons, San Gabriel Mountains, California, and implications for the geologic history of the San Gabriel terrane. *Mem. Geol. Soc. Am.*, **174,** 33–45.

Barth, A.P. & May, J.D. (1992) Mineralogy and pressure-temperature-time path of the Cretaceous granulite gneisses, south-eastern San Gabriel Mountains, southern California. *J. Metamorphic Geol.*, **10,** 529–544.

Barth, A.P., Wooden, J.L., Tosdal, R.M., Morrison, J., Dawson, D.L. & Hernly, B.M. (1995) Origin of gneisses in the aureole of the San Gabriel anorthosite complex and implications for the Proterozoic crustal evolution of southern California. *Tectonics*, **14,** 736–752.

Brandon, M.T., Roden-Tice, M.K. & Garver, J.I. (1998) Late Cenozoic exhumation of the Cascadia accretionary wedge in the Olympic Mountains, northwest Washington State. *Bull. Geol. Soc. Am.*, **110,** 985–1009.

Brown, R. (1991) Backstacking apatite fission-track 'stratigraphy': a method for resolving the erosional and isostatic rebound components of tectonic uplift histories. *Geology*, **19,** 74–77.

Burbank, D.W., Leland, J., Fielding, E., Anderson, R.S., Brozovic, N., Reid, M.R. & Duncan, C. (1996) Bedrock incision, rock uplift and threshold hillslopes in the northwestern Himalayas. *Nature*, **379,** 505–510.

Carlson, W.D. (1990) Mechanisms and kinetics of apatite fission track annealing. *Am. Miner.*, **75,** 1120–1139.

Carlson, W.D., Donelick, R.A. & Ketcham, R.A. (1999) Variability of apatite fission-track annealing kinetics: I. Experimental results. *Am. Miner.*, **84,** 1213–1223.

Corrigan, J. (1991) Inversion of apatite fission track data for thermal history information. *J. geophys. Res.*, **96,** 10347–10360.

Crook, R. Jr, Allen, C.R., Kamb, B., Payne, C.M. & Proctor, R.J. (1987) Quaternary geology and seismic hazard of the Sierra Madre and associated faults, western San Gabriel Mountains. In: *Recent Reverse Faulting in the Transverse Ranges, California* (Ed. by D. M. Morton & R. F. Yerkes), *U.S. Geol. Surv. Prof. Paper*, **1339,** 27–64.

Crouch, J.K. & Suppe, J. (1993) Late Cenozoic tectonic evolution of the Los Angeles basin and inner California borderland: a model for core complex-like crustal extension. *Bull. Geol. Soc. Am.*, **105,** 1415–1434.

Crowell, J.C. (1975) The San Gabriel Fault and Ridge Basin. In: *The San Andreas Fault in Southern California* (Ed. by J. C. Crowell), *California Division of Mines and Geology Special Report*, **118,** 223–233.

Crowell, J.C. (1982) The tectonics of the Ridge basin, southern California. In: *Geologic History of Ridge Basin, Southern California* (Ed. by M. H. Link & J. C. Crowell), 25–42. Soc. Econ. Paleo. Mineral., Pacific Section.

Crowley, K.D., Cameron, M. & Schaeffer, R.L. (1991) Experimental studies of annealing of etched fission tracks in fluorapatite. *Geochim. Cosmochim. Acta*, **55,** 1449–1465.

Demets, C. (1995) Reappraisal of seafloor spreading lineations in the Gulf of California: Implications for the transfer of Baja California to the Pacific Plate and estimates of Pacific-North America motion. *Geophys. Res. Lett.*, **22,** 3545–3548.

Dibblee, T.W. Jr (1982) Regional geology of the Transverse Ranges province of Southern California. In: *Geology and Mineral Wealth of the California Transverse Ranges* (Ed. by D. L. Fife & J. L. Minch), pp. 27–39. South Coast Geological Society, Inc.

Dickinson, W.R. (1996) Kinematics of transrotational tectonism in the California Transverse Ranges and its contribution to cumulative slip along the San Andreas transform fault system. *Geol. Soc. Am. Special Paper*, **305,** 1–46.

Dolan, J.D., Jordan, F., Rasmussen, G., Stevens, D., Reeder, W. & McFadden, L.M. (1996) Evidence for probable moderate-sized (Mw 6.5–7.0) paleoearthquakes on the Cucamonga fault, northwestern Los Angeles metropolitan region, California [abs.]. *EOS Transactions, A.G.U.*, **77,** F460.

Dumitru, T.A. (1993) A new computer automated microscope stage system for fission-track analysis. *Nuclear Tracks Radiation Measurements*, **21,** 575–580.

Dumitru, T.A., Gans, P.B., Foster, D.A. & Miller, E.L. (1991) Refrigeration of the western Cordillera lithosphere during Laramide shallow-angle subduction. *Geology*, **19,** 1145–1148.

Ehlig, P.L. (1975) Basement rocks of the San Gabriel

Mountains, south of the San Andreas fault, southern California. *California Div. Mines Geol. Special Report*, **118,** 177–186.

Ehlig, P.L. (1981) Origin and tectonic history of the basement terrane of the San Gabriel Mountains, Central Transverse Ranges. In: *The Geotectonic Development of California* (Ed. by W. G. Ernst), pp. 253–283. Prentice Hall, Inc., Edgewood Cliffs, NJ.

Farley, K.A., Wolfe, R.A. & Silver, L.T. (1996) The effects of long alpha-stopping distances on (U-Th) /He dates. *Geochim. Cosmochim. Acta*, **60,** 4223–4229.

Fitzgerald, P.G., Sorkhabi, R.B., Redfield, T.F. & Stump, E. (1995) Uplift and denudation of the central Alaska Range: a case study in the use of apatite fission track thermochronology to determine absolute uplift parameters. *J. geophys. Res.*, **100,** 20175–20191.

Foster, D.A., Gleadow, A.J.W., Reynolds, S.J. & Fitzgerald, P.G. (1993) Denudation of metamorphic core complexes and the reconstruction of the Transition Zone, west central Arizona: Constraints from apatite fission track thermochronology. *J. geophys. Res.*, **98,** 2167–2185.

Foster, D.A., Miller, D.S. & Miller, C.F. (1991) Tertiary extension in the Old Woman Mountains area, California: evidence from apatite fission track analysis. *Tectonics*, **10,** 875–886.

Galbraith, R.F. (1981) On statistical models for fission track counts. *J. International Assoc. Math. Geol.*, **13,** 471–488.

Galbraith, R.F. & Laslett, G.M. (1993) Statistical models for mixed fission track ages. *Nucl. Tracks Radiat. Meas.*, **21,** 459–470.

Gallagher, K. (1995) Evolving temperature histories from apatite fission-track data. *Earth planet. Sci. Lett.*, **136,** 421–435.

Gleadow, A.J.W. & Duddy, I.R. (1981) A natural long-term annealing experiment for apatite. *Nuclear Tracks*, **5,** 169–174.

Gleadow, A.J.W., Duddy, I.R., Green, P.F. & Lovering, J.F. (1986) Confined fission track lengths in apatite: a diagnostic tool for thermal history analysis. *Contrib. Miner. Petrol.*, **94,** 405–415.

Gleadow, A.J.W., Duddy, I.R. & Lovering, J.F. (1983) Fission track analysis: a new tool for the evaluation of thermal histories and hydrocarbon potential. *Australia Petrol. Expl. Assoc. J.*, **23,** 93–102.

Gleadow, A.J.W. & Fitzgerald, P.G. (1987) Uplift history and structure of the Transantarctic Mountains: New evidence from fission track dating of basement apatites in the Dry Valleys area, southern Victoria Land. *Earth planet. Sci. Lett.*, **82,** 1–14.

Green, P.F. (1981) A new look at statistics in fission track dating. *Nuclear Tracks Radiation Measurements*, **5,** 77–86.

Green, P.F., Duddy, I.R., Gleadow, A.J.W., Tingate, P.R. & Laslett, G.M. (1986) Thermal annealing of fission tracks in apatite: 1 – a qualitative description. *Chem. Geol. (Isotope Geoscience Section)*, **59,** 237–253.

Green, P.F., Duddy, I.R., Laslett, G.M., Hegarty, K.A., Gleadow, A.J.W. & Lovering, J.F. (1989) Thermal annealing of fission track in apatite 4. Qualitative modelling techniques and extensions to geological timescales. *Chem. Geol. (Isotope Geoscience Section)*, **79,** 155–182.

Grove, M. & Lovera, O. (1996) Slip-History of the Vincent Thrust: Role of denudation during shallow subduction. In: *Subduction: Top to Bottom, Am. Geophys. Union, Geophys. Monograph*, **96,** 163–170.

Hadley, D. & Kanamori, H. (1976) Seismic structure of the Transverse Ranges, California. *Bull. Geol. Soc. Am.*, **88,** 1469–1478.

Hazelton, G.B. & Nourse, J.A. (1994) Constraints on the direction of Miocene extension and degree of crustal tilting in the eastern San Gabriel Mountains, southern California. *Geol. Soc. Am. Abstracts with Programs*, **26,** 58.

House, M.A., Farley, K.A. & Kohn, B.P. (1999) An empirical test of helium diffusion in apatite: borehole data from the Otway basin, Australia. *Earth planet. Sci. Lett.*, **170,** 463–474.

Hurford, A.J. & Green, P.F. (1983) The Zeta age calibration of fission-track dating. *Isotope Geoscience*, **1,** 285–317.

Ingersoll, R.V. & Rumelhart, P.E. (1999) Three-stage evolution of the Los Angeles basin, southern California. *Geology*, **27,** 593–596.

Jacobsen, C.E. (1990) The $^{40}Ar/^{39}Ar$ geochronology of the Pelona Schist and related rocks, Southern California. *J. Geophys. Res.*, **95,** 509–528.

Jacobsen, C.E., Dawson, M.R. & Postlethwaite, C.E. (1988) Structure, metamorphism, and tectonic significance of the Pelona, Orocopia, and Rand schists, southern California. In: *Metamorphism and Crustal Evolution in the Western United States* (Ed. by W. G. Ernst), pp. 976–997. Prentice Hall, Englewood Cliffs, New Jersey.

Jennings, C.W. (1977) Geologic Map of California. *California Div. Mines Geol, 1 Sheet, Scale, 1:750,000.*

Jennings, C.W. & Strand, R.G. (1991) Geologic Map of California. *Los Angeles Sheet, California Div. Mines Geol, 1 Sheet, Scale, 1:250,000.*

Ketcham, R.A., Donelick, R.A. & Carlson, W.D. (1999) Variability of apatite fission-track annealing kinetics: III. Extrapolation to geological time scales. *Am. Miner.*, **84,** 1235–1255.

Laslett, G.N., Green, P.F., Duddy, I.R. & Gleadow, A.J.W. (1987) Thermal annealing of fission tracks in apatite, 2, A quantitative analysis. *Chem. Geol. (Isotope Geoscience Section)*, **65,** 1–13.

Li, Y.-G., Henyey, T.L. & Leary, P.C. (1992) Seismic reflection constraints on the structure of the crust beneath the San Bernardino Mountains, Transverse Ranges, southern California. *J. Geophys. Res.*, **97,** 8817–8830.

Mancktelow, N.S. & Grasemann, B. (1997) Time-dependent effects of heat advection and topography on cooling histories during erosion. *Tectonophysics*, **270,** 167–195.

May, S.R. & Repenning, C.A. (1982) New evidence for the age of the Old Woman sandstone, Mojave Desert, California. In: *Late Cenozoic Stratigraphy and Structure of the San Bernardino Mountains* (Ed. by M. Sadler & M. A. Kooser), *Geol. Soc. Am. Cordilleran Section Field Trip Guidebook*, **6,** 75–81.

May, S.R. & Walker, N.W. (1989) Late Cretaceous juxtaposition of metamorphic terranes in the southeastern San Gabriel Mountains, California. *Bull. Geol. Soc. Am.*, **101,** 1246–1267.

Meigs, A.J., Brozovic, N. & Johnson, M. (1999) Steady balanced rates of uplift and erosion of the Santa Monica Mountains, California. *Basin Res.*, **11,** 59–74.

Meisling, K.E. (1984) Neotectonics of the north frontal fault system of the San Bernardino Mountains: Cajon Pass to Lucerne Valley, California. *PhD Thesis*, Calif. Inst. of Technol., Pasadena, California.

Meisling, K.E. & Weldon, R.J. (1989) Late Cenozoic tectonics

of the northwestern San Bernardino Mountains, southern CA. *Bull. Geol. Soc. Am.*, **101,** 106–128.

Miller, F.K. & Morton, D.M. (1977) Comparison of granitic intrusions in the Pelona and Orocopia Schists, southern California. *U.S. Geol. Surv. J. Res.*, **5,** 643–649.

Molnar, P. & England, P. (1990) Late Cenozoic uplift of mountain ranges and global climatic change: chicken or egg? *Nature*, **346,** 29–34.

Naeser, C.W. (1976) Fission Track Dating. *U.S. Geol. Surv. Open-File Report*, 76–109.

Naeser, C.W. (1979) Fission-track dating and geologic annealing of fission tracks. In: *Lectures in Isotope Geology* (Ed. by E. Jäger & J. C. Hunziker), pp. 154–169. Springer-Verlag, New York.

Naeser, C.W. & Faul, H. (1969) Fission track annealing in apatite and sphene. *J. geophys. Res.*, **74,** 705–710.

Nilsen, T.H. (1987) Paleogene tectonics and sedimentation of coastal California. In: *Cenozoic Basin Development of Coastal California* (Ed. by R. V. Ingersoll & W. G. Ernst.), IV, pp. 81–123. Prentice Hall, Inc., Englewood Cliffs, NJ.

Oberlander, T.M. (1972) Morphogenesis of granitic boulder slopes in the Mojave desert, California. *J. Geol.*, **80,** 1–20.

Pinet, P. & Souriau, M. (1988) Continental erosion and large-scale relief. *Tectonics*, **7,** 563–582.

Ryberg, T. & Fuis, G.S. (1998) The San Gabriel Mountains bright reflective zone: possible evidence of young mid-crustal thrust faulting in southern California. *Tectonophysics*, **286,** 31–46.

Sadler, P.M. (1982) Provenance and structure of late Cenozoic sediments in the northeast San Bernardino Mountians. In: *Geologic Excursions in the Transverse Ranges* (Ed. by J. D. Cooper), *Geol. Soc. Am. Cordilleran Section, Field Trip Guidebook*, **6,** 83–91.

Sadler, P.M. (1993) The Santa Ana basin of the central San Bernardino Mountains: Evidence of the timing of uplift and strike-slip relative to the San Gabriel Mountains. In: *The San Andreas Fault System: Displacement, Palinspastic Reconstruction, and Geologic Evolution* (Ed. by R. E. Powell, R. J. Weldon & J. C. Matti), *Geol. Soc. Am. Memoir*, **178,** 307–321.

Sadler, P.M. & Reeder, W.A. (1983) Upper Cenozoic, quartzite-bearing gravels of the San Bernardino Mountains, Southern California: Recycling and mixing as a result of transpressional uplift. In: *Tectonics and Sedimentation Along Faults in the San Andreas System* (Ed. by D. W. Anderson & M. J. Rymer), pp. 45–57. Pacific Section, Soc. Econ. Paleontologists and Mineralogists.

Savage, J.C. & Lisowski, M. (1994) Strain accumulation north of Los Angeles, California, as a function of time. 1977–92. *Geophys. Res. Lett.*, **21,** 1173–1176.

Savage, J.C., Prescott, W.H. & Gu, G. (1986) Strain accumulation in southern California. 1973–84. *J. geophys. Res.*, **91,** 7455–7473.

Schmidt, K.M. & Montgomery, D.R. (1995) Limits to relief. *Science*, **270,** 617–620.

Scott, R.J., Foster, D.A. & Lister, G.S. (1998) Tectonic implications of rapid cooling of lower plate rocks from the Buckskin-Rawhide metamorphic core complex, west-central Arizona. *Bull. Geol. Soc. Am.*, **110,** 588–614.

Seeber, L. & Armbruster, J.G. (1995) The San Andreas fault system through the Transverse Ranges as illuminated by earthquakes. *J. geophys. Res.*, **100,** 8285–8310.

Spotila, J.A., Farley, K.A. & Sieh, K. (1998) Uplift and erosion of the San Bernardino Mountains associated with transpression along the San Andreas fault, California, as constrained by radiogenic helium thermochronometry. *Tectonics*, **17,** 360–378.

Stüwe, K., White, L. & Brown, R. (1994) The influence of eroding topography on steady-state isotherms. Application to fission track analysis. *Earth Planet. Sci. Lett.*, **124,** 63–74.

Sugai, T. & Ohmori, H. (1999) A model of relief forming by tectonic uplift and valley incision in orogenesis. *Basin Res.*, **11,** 43–58.

Terres, R.R. & Luyendyk, B.P. (1985) Neogene tectonic rotation of the San Gabriel region, California, suggested by paleomagnetic vectors. *J. geophys. Res.*, **90,** 12467–12484.

Tippett, J.M. & Kamp, P.J.J. (1995) Quantitative relationships between uplift and relief parameters for the Southern Alps, New Zealand, as determined by fission track analysis. *Earth Surf. Process. Landforms*, **20,** 153–175.

Wagner, G.A. (1968) Fission track dating of apatites. *Earth Planet. Sci. Lett.*, **4,** 411–415.

Walls, C., Rockwell, T., Pfanner, J., Bornyasz, M. & Lindvall, S. (1997) Uplift gradient along the Sierra Madre – Cucamonga fault zone, Los Angeles, California. *Geol. Soc. Am. Cordillera Section, Abstracts with Program*, **29,** 72.

Webb, T.H. & Kanamori, H. (1985) Earthquake focal mechanisms in the eastern Transverse Ranges and San Emigdio Mountains, southern California and evidence for a regional detachment. *Bull. Seism. Soc. Am.*, **75,** 737–757.

Willett, S.D. (1997) Inverse modelling of annealing of fission tracks in apatite 1: a controlled random search method. *Am. J. Sci.*, **297,** 939–969.

Wolf, R.A., Farley, K.A. & Silver, L.T. (1996) Helium diffusion and low temperature thermochronometry of apatite. *Geochim. Cosmochim. Acta*, **60,** 4231–4240.

Wolf, R.A., Farley, K.A. & Silver, L.T. (1997) Assessment of (U-Th) /He thermochronometry: the low-temperature history of the San Jacinto mountains, California. *Geology*, **25,** 64–68.

Wright, T.L. (1987) Geologic evolution of the petroleum basins of southern California. In: *Petroleum Geology of Coastal Southern California* (Ed. by T. Wright & R. Heck), pp. 1–19. Pacific Section, Am. Assoc. Petroleum Geologists, Los Angeles.

Wright, T.L. (1991) Structural geology and tectonic evolution of the Los Angeles basin, California. In: *Active Margin Basins* (Ed. by K. T. Biddle), *Am. Assoc. Petroleum Geologists Memoir*, **52,** 35–134.

Yeats, R.S. (1981) Quaternary flake tectonics of the California Transverse Ranges. *Geology*, **10,** 363–376.

Received 16 July 1999; revision accepted 8 May 2000